Viscosity of Nanoconfined Polyamide-6,6 Oligomers: Atomistic Reverse Nonequilibrium Molecular Dynamics Simulation

Hossein Eslami*,†,‡ and Florian Müller-Plathe†

Eduard-Zintl Institut für Anorganische und Physikalische Chemie, Technische Universität Darmstadt, Petersenstrasse 20, D-64287, Germany, and Department of Chemistry, College of Sciences, Persian Gulf University, Boushehr 75168, Iran

Received: September 8, 2009; Revised Manuscript Received: October 20, 2009

Our new simulation scheme in isosurface−isothermal−isobaric ensemble [Eslami, H.; Mozaffari, F.; Moghadasi, J.; Müller-Plathe, F. *J. Chem. Phys.* **2008**, *129*, 194702], developed to simulate confined fluids in equilibrium with bulk, is applied to simulate polyamide-6,6 oligomers confined between graphite surfaces. The reverse nonequilibrium molecular dynamics simulation technique is employed to shear the graphite surfaces. In this work, six confined systems, with different surface separations, as well as the bulk fluid are simulated. Our results show a viscosity increase with respect to the bulk fluid, with decreasing distance between surfaces. Also, the calculated viscosities of the confined systems show an oscillatory behavior with maxima corresponding to well-formed layers between the surfaces. We observe a substantial slip at the surfaces, with the slip length depending on the shear rate and on the slit width. The slip length and the slip velocity show oscillatory behavior with out-of-phase oscillations with respect to the solvation force oscillations. Moreover, the temperature difference between coldest and hottest parts of the simulation box depends on the shear rate and on the layering effect (solvation force oscillations). An analysis of oligomer deformation under flow shows preferential alignment of oligomers parallel to the surfaces with increasing shear rate.

Introduction

In our earlier paper[1] we investigated the structure and mobility of nanoconfined polyamide-6,6 (PA-6,6) oligomers confined between graphite surfaces. As the continuation of that work, in this paper we investigate the rheological properties of nanoconfined polymers, which are of fundamental importance in such industrial applications as lubrication, polymer processing, adhesion, friction, wear, protective coatings, paints, and layered polymer composites.[2,3] For example, for applying thin polymer films for such purposes as solid lubrication,[4,5] or in applications involving sliding of rubber components,[6,7] the tribological properties of polymers are of prime importance. Also, soluble polymers are added to almost all multigrade engine oils as viscosity modifiers, to control the rheological properties of the fluids with which they are blended.[8] Therefore, understanding the basic mechanism behind the polymer friction is of importance in understanding the above-cited phenomena.

It is well-known that, on confining a fluid in a nanometric pore, the density profiles show a strong layered structure.[1,9−18] Strong density fluctuations near the confining surfaces result in the deviation of transport properties from their corresponding bulk properties.[19−21] For example, it has been shown that, for a fluid in confinement, a deviation from typical quadratic velocity profiles predicted by classical Navier−Stokes theory is observed for planar Poiseuille flow.[22] These findings indicate that the common treatments used for liquids are not generally valid for investigation of fluids in confinement; rather, they have to be reconsidered to explicitly account for the new boundary conditions, interactions at the solid−liquid interface, and other factors which may characterize confined fluids. To rationalize rheological and tribological mechanisms, the atomic-level origins of friction have been investigated, both experimentally and theoretically.

New experimental techniques, such as surface force apparatus and atomic force microscopy, have been used to study molecular- and atomic-level rheology and tribology.[23−26] The former technique provides information on the structural and rheological properties of thin molecular films,[23−26] such as surface-induced phase transitions, viscosity change, and quantized frictional forces. Improvements in surface force apparatus techniques have made it possible to measure precisely the normal and tangential components of the pressure when sliding the two surfaces under compression. These experiments are of considerable importance in understanding the lubrication process. So far, extensive experimental work has focused on the friction response of simple liquids or liquidlike lubricants sliding under steady state conditions.[27−32] Friction has been measured for thin films confined between mica, cobalt, and carbon surfaces. A recent review of the experimental techniques used to study lubrication and diffusion of polymers at surfaces was given by Bae and Granick.[33] While the results of such studies show strong deviations from the bulk in the tracer diffusion coefficients, the local viscosity, and the mechanical properties of confined polymers with respect to the bulk polymer, they reveal that the topography of the surfaces as well as the contact area determine the friction force.[34,35]

From a theoretical point of view, viscous flow is historically investigated using principles of classical fluid dynamics, in which the fluid flow is treated using a macroscopic approach.[36] Improvements in this field were made through solving flow problems by numerical simulation: the so-called computational fluid dynamics.[36] Although this method has widely been applied in solving dynamic systems under flow, fluid dynamics does not account for any interaction between individual atoms or

* Corresponding author. E-mail: h.eslami@theo.chemie.tu-darmstadt.de.
† Technische Universität Darmstadt.
‡ Persian Gulf University.

10.1021/jp908659w
Published on Web 11/10/2009

molecules. As a result, such extreme conditions as fluid behavior at walls and other rheological phenomena cannot be simulated accurately on a macroscopic scale. On the other hand, experimental measurements, as described in the preceding paragraph, are very difficult to perform, due to the existence of only a small amount of material in the confined region. Besides, the transport properties of thin films, measured experimentally, reflect the combined effects of various parameters such as the orientation, the packing, and the interaction of molecules, and it is still very difficult to determine all properties such as boundary conditions and fluid properties by experimental measurement.[37] Therefore, in spite of large body of experimental measurements, the properties of confined fluids are still far from being fully understood.

Molecular simulation methods, on the other hand, have provided most of the microscopic information on the molecular understanding of confined fluids.[1,9−18] The molecular dynamics (MD) method has been used to investigate the behavior of simple fluids under shear.[9,38−46] There are, however, only a few reports in the literature on the MD simulation of confined chain molecules or polymers under flow. Here we briefly review some of these works and the main conclusions found in their studies. In their simulation of slip on the wall, Thompson and Robbins[41] and Thompson et al.[42] used a bead−spring model for linear chain molecules of varying chain lengths and observed significant slip that depended on many factors such as the fluid−wall interaction energy and shear rate. Manias et al.[47,48] used the same bead−spring model to calculate the viscosity inside the solid−fluid interface. They found that nearly all the shear thinning takes place inside the solid−fluid interface and the shear thinning inside the interfacial area is determined by the wall affinity.[47,48] Confined bead−spring polymer melts in a shear flow were studied, using MD simulations, by Khare et al.,[45,46,49] in which they found a viscosity increase with decreasing film thickness. MD simulations of united atom models of hexadecane under flow, confined between fcc (111), graphite, and bcc surfaces, have been carried out by Stevens et al.,[50] by Balasundaram et al.,[51] and by Jabbarzadeh et al.,[37,52−56] respectively, in which the effects of surface roughness, hydrocarbon branching, and shear rate on the density and the viscosity coefficient have been studied. A similar study on the united atom model of confined *n*-dodecane has been performed by Gui et al.,[57] and a substantial slip at the wall and an essentially constant velocity over most of the interior space between the walls have been observed. Other studies consist of MD simulations of bead−spring polymer models to study the behavior of polymer melts under flow, for example, Jeng et al.,[58] Müller et al.,[59] and Zhang et al.[60] Dissipative particle dynamics simulation of polymer brushes under shear was done by Goujon et al.[61]

The type of experiments we are interested in mimicking are the surface force apparatus experiments, in which the fluid is confined between two surfaces separated on the order of nanometers and moving relative to each other.[23−26] The viscosity is therefore calculated from experimental measurements of the shear stress and the applied shear rate, which in turn is determined by assuming a linear velocity profile between the surfaces. Recently, we have developed a new MD simulation method of confined fluids at a constant number of confined particles, N, constant surface area, A, constant temperature, T, and constant parallel component of the pressure, $P_{||}$, which we call *NAPT* ensemble simulation hereafter.[62] The simulation has been shown to mimic surface force apparatus experiments and has been applied to the case of thin films of PA-6,6 confined between two parallel graphite surfaces.[1] In this work, we extend this simulation method to calculate the shear viscosity coefficient of PA-6,6 oligomers confined between graphite surfaces using the reverse nonequilibrium molecular dynamics (RNEMD) simulation technique. The motivations for this study stem from the following: (1) In many of the existing simulation methods in the literature, the temperature is kept constant uniformly across the entire fluid film. The objection to these methods is that the generated viscous heat is artificially removed by the thermostat. The RNEMD simulation method employed in this work[63] is shown to conserve both total energy and the total linear momentum of the system, and hence, it does not require a thermostat. Even if a thermostat is used for practical purposes, it has been shown that the calculated viscosities using RNEMD are not sensitive to the choice of the thermostat coupling time.[63,64] (2) Most of the existing simulations in the literature do not mimic the surface force apparatus experiments, because on performing equilibrium simulations the fluid in the confined region is not in equilibrium with the bulk phase, which necessitates either performing simulations in the grand canonical ensemble (GCE) or explicitly including the bulk fluid in the simulation box. Our new *NAPT* simulation method[62] was shown to reproduce the results of GCE simulation method,[65−69] which guarantees the existence of equilibrium between the fluid in the confined region and the bulk fluid. (3) In almost all the reports in the literature on transport properties of confined polymers, as addressed above, a bead−spring model is used to describe the polymer matrix and simulation studies of confined realistic polymers are scarce. Just in some cases more realistic united atom models of flexible chains, like alkanes, are studied. However, atomistic simulation reports on polymers consisting of stiff chains under flow are scarce.

Method

In the scope of linear-response theory, a flux (momentum) is related to a thermodynamic driving force (velocity gradient) and the proportionality constant is a transport coefficient (viscosity). The velocity gradient, also called the shear rate, γ, field is a gradient of one component of the fluid velocity, say the x direction, with respect to another direction, say the z direction, i.e.

$$\gamma = \frac{\mathrm{d}v_x(z)}{\mathrm{d}z} \tag{1}$$

The momentum flux $j_z(p_x)$ is collinear: It is the x-component of the momentum p_x transported in the z direction through a perpendicular surface of area A per time t. It can also be regarded as an off-diagonal (xz) component of the stress tensor. The proportionality coefficient is the shear viscosity, η.

$$j_z(p_x) = -\eta \frac{\partial v_x}{\partial z} \tag{2}$$

Transport coefficients can be calculated using equilibrium[70] or nonequilibrium[71] MD simulations, in which an appropriate perturbation is applied and the ensemble average of the resulting flux is measured.

In a series of articles by Müller-Plathe et al.[63,72,73] the RNEMD technique is established, in which the flux is imposed and the corresponding force is measured. It is called "reverse" because the cause and effect are reversed with respect to experiment and the conventional nonequilibrium simulation methods. The

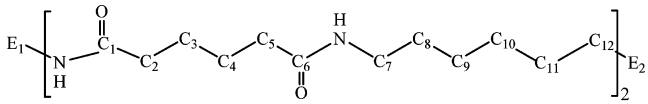

E_1=C_2H_5

E_2=$NHCO(CH_2)_4CONHC_4H_9$

Figure 1. Chemical structure of PA-6,6 oligomer studied in this work.

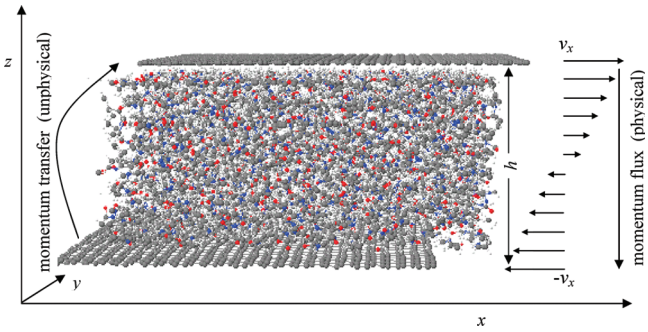

Figure 2. Snapshot of the simulation box. The distance between graphene surfaces is h (the upper and lower confining surfaces are located at $z = h/2$ and $z = -h/2$, respectively). The arrows show the x-component of velocities of slabs along the z direction.

method has been successfully extended to simulate molecular fluids,[72,73] complex fluids,[74,75] polymers,[76,77] and ionic liquids.[78] Here we briefly describe the basic elements of the method, with the main emphasis on confined fluids. The confined fluid is a melt of PA-6,6 oligomers, studied in our former work,[1] for which the chemical structure is shown in Figure 1, and the confining surfaces are graphene monolayers. The simulation box is periodic in the x and y directions, but not in the z direction. The graphene surfaces are separated by a distance h in the z direction and the unphysical momentum transfer is imposed between the surfaces; i.e, the graphene surfaces are sheared with respect to each other. A snapshot of a simulation box is shown in Figure 2. The periodic box is subdivided into slabs in the z direction, perpendicular to the surfaces (see Figure 2). The momentum flux is imposed on the system in an unphysical way, as follows. The atoms moving against the desired surface movement are found. In the graphene surface moving in the $+x$ direction (upper surface at $z = +h/2$), the carbon atom with the largest momentum component in the $-x$ direction (the atom with the smallest p_x) is found. Likewise, in the graphene surface moving in the $-x$ direction (lower surface at $z = -h/2$), the carbon atom with the largest momentum component in the $+x$ direction (the atom with the largest p_x) is found. Then the p_x's of the two atoms are swapped. Here the surface atoms all have the same mass; therefore the unphysical momentum swap conserves both the linear momentum and the kinetic energy of the system as a whole. Since the positions of the atoms are not changed, the potential energy and hence the total energy of the system are conserved.

In this method, the amount of momentum Δp_x transferred from the surface moving in the $-x$ direction to that moving in the $+x$ direction is precisely known. Therefore, periodically repeating momentum swaps, the total momentum transferred in a simulation is known as the sum of the Δp_x. The physical momentum flow, in the opposite direction, occurs in the system as the result of system response to nonequilibrium situation. In the steady state, the rate of momentum transferred unphysically by momentum swaps is equal to that of momentum flowing back through the fluid by friction. Hence, the momentum flux $j_z(p_x)$ can be calculated.

$$j(p_x) = \frac{P_x}{At} \tag{3}$$

where P_x is the total momentum transferred in time t of simulation and A is the surface area. Therefore a uniform velocity profile will develop in the fluid as the result of physical momentum flux (see Figure 2). The mean flow velocity v_x in each slab can be easily obtained by averaging the x-component of velocities of its constituent atoms. Given that the response of the system to the perturbation is linear, a linear velocity profile will be obtained and the average $\langle \partial v_x/\partial z \rangle$ can be obtained by a linear regression.

In this work our new *NAPT* ensemble simulation technique[62] is employed to simulate confined PA-6,6 oligomers confined between graphene surfaces, in equilibrium with bulk sample. The RNEMD technique[63,72−78] is then used to shear the graphene surfaces with respect to each other to calculate the viscosity coefficient of the confined fluid as a function of separation between surfaces. The effect of solvation force on the viscosity coefficient and the structural changes in the presence of flow are also investigated.

Simulation Details

Similar to the former work,[1] atomistic MD simulations were performed for ethyl- and butyl-terminated PA-6,6 trimers, whose chemical structures are shown in Figure 1. The force field parameters for PA-6,6 as well as for the confining surfaces, graphene surfaces, are reported in our former publication.[1] The parameters for unlike interactions were determined using Lorentz−Berthelot mixing rules.[70] Six confined systems as well as the bulk fluid are simulated in this work (Table 1). The widths of the confined systems were selected to be able to study systems with highly repulsive and attractive solvation forces. Because PA-6,6 is highly viscous and the confined fluid has an even higher viscosity than the bulk, simulations were performed at a higher temperature, 500 K, to be able to obtain results in a few tens of nanoseconds.

All MD simulations were carried out using our simulation package, YASP.[79,80] Nonbonded interactions were applied fully between atoms interacting through torsion terms (one to four interactions). All nonbonded interactions were truncated at 0.95 nm with a reaction field correction for the Coulombic interactions.[70] The effective dielectric constant was taken to be 5.5.[81,82] An atomic Verlet neighbor list was used, which was updated every 15 time steps, and the neighbors were included if they were closer than 1.0 nm. The time step for the leapfrog integration scheme[70] was 1.0 fs. After an equilibration of 3 ns, in *NAPT* ensemble simulation for the systems described in Table 1, relaxed configurations were obtained for performing RNEMD simulation. The details of the *NAPT* ensemble simulation are given elsewhere;[62] here we restrict ourselves to a short description of basic elements of the method. In this method the temperature is kept fixed using a Berendsen thermostat,[83] and the parallel component of pressure, $P_{||}$, defined as

$$P_{\parallel} = \frac{P_{xx} + P_{yy}}{2} = \frac{1}{3V}\sum_i m_i v_i^2 + \frac{1}{2V}[\sum_i \sum_j (\mathbf{X}_{ij} \cdot \mathbf{F}_{x,ij} + \mathbf{Y}_{ij} \cdot \mathbf{F}_{y,ij}) + \sum_i \sum_s (\mathbf{X}_{is} \cdot \mathbf{F}_{x,is} + \mathbf{Y}_{is} \cdot \mathbf{F}_{y,is})] + \frac{1}{2V}[\sum_s \sum_t (\mathbf{X}_{st} \cdot \mathbf{F}_{x,st} + \mathbf{Y}_{st} \cdot \mathbf{F}_{y,st})] \quad (4)$$

is kept fixed by coupling $P_{\parallel}$ to a Berendsen barostat, as explained elsewhere.[62] Here, P_{xx} and P_{yy} are the x- and y-components of the pressure tensor, respectively, m is the atomic mass, V is the volume, subscripts i and j show the atoms in the confined region, subscripts s and t stand for the surface atoms, $\mathbf{X}$ and $\mathbf{Y}$ are the relative distances between particles in the x and y directions, respectively, and $\mathbf{F}_x$ and $\mathbf{F}_y$ are their corresponding forces. In fact, in this method $P_{\parallel}$ is kept fixed (to the bulk pressure) by changing the distance between the confining surfaces. The method is shown to simulate the surface force apparatus experiment[23,24] and the results generated using this method have been validated against the GEC simulation results[66−69] and also against the simulation results in which the fluid in confinement is in equilibrium with the bulk fluid.[17]

In this work, the temperature and the $P_{\parallel}$ were kept fixed at 500 K and at 101.3 kPa, respectively, with the method described above.[1,62] The temperature and pressure coupling constants were 0.2 ps and 5.0 ps, respectively. Having prepared a relaxed configuration for each system, RNEMD simulations were performed, using the afore-cited method. The results are explained in the following section.

Results and Discussion

Local Density Profiles and Solvation Force Oscillations. Similar to the former work,[1] the distribution of mass density of all atoms as a function of their distances with respect to the confining surfaces are shown in Figure 3. Here the distance between the surfaces, h, is divided into a number of thin slabs and the time-averaged density for each slab is calculated during the simulation. The results show that confined oligomers form layered structures near the surfaces and, with changing the ratio of number of oligomers to the surface area (see Table 1) at a constant bulk pressure, $P_{\parallel} = 101.3$ kPa, the number of well-formed layers between surfaces is changing. At surface separations of around 4.0 nm the local density shows four peaks in the vicinity of each surface and the intermediate region does not show a layering effect. In this region the local density has a mean value corresponding to the bulk liquid density.

The solvation force, f_s, which is the force that would be required to keep the surfaces at a fixed distance, is defined in terms of parallel and perpendicular components of pressure as

$$\langle f_s \rangle = A(\langle P_{\perp} \rangle - \langle P_{\parallel} \rangle) \quad (5)$$

where $P_{\perp}$ is the perpendicular component of pressure and brackets indicate the average. Shown in Figure 4 is the average solvation force per unit area, versus average surface separation, $\langle h \rangle$. The period of oscillations in the solvation force is equal to the period of formation/deformation of layers. As shown in the former work,[1] better layered structures with sharper density peaks correspond to more repulsive solvation forces. The oscillations in the solvation force curve correspond to the ordering/disordering of formed layers parallel to the surfaces.

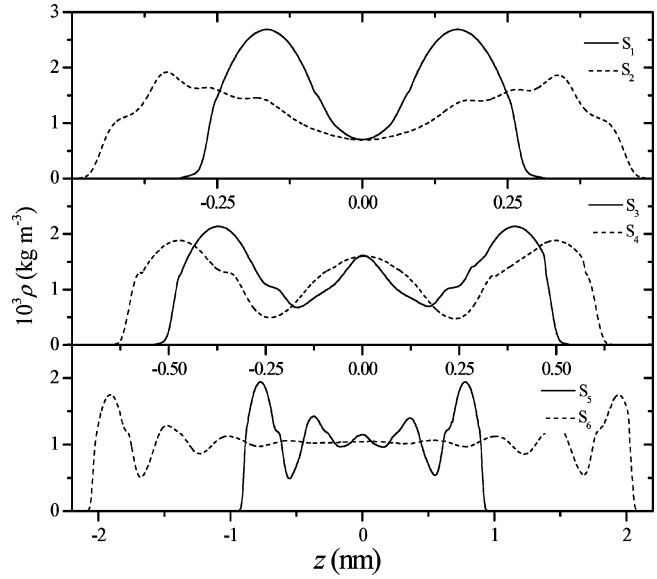

Figure 3. Local density profiles for systems S_1-S_6 at $T = 500$ K and $P_{\parallel} = 101.3$ kPa. The number of oligomers, surface area, and average surface separations are given in Table 1.

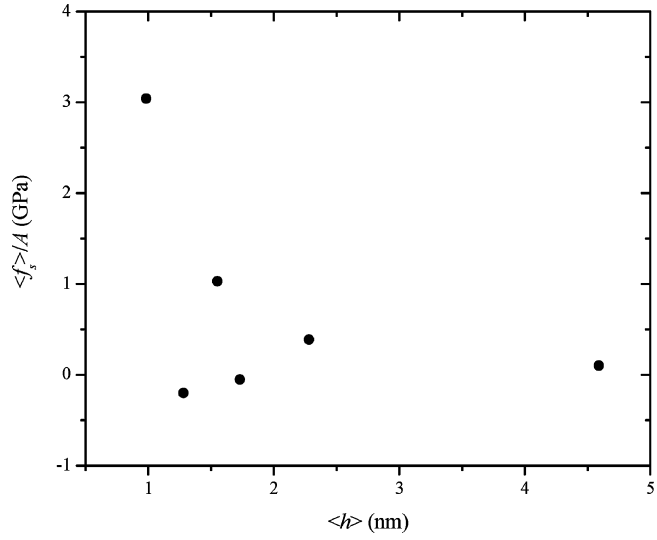

Figure 4. Calculated solvation force as a function of average surface separation, $\langle h \rangle$, for systems S_1-S_6, at $T = 500$ K and $P_{\parallel} = 101.3$ kPa.

TABLE 1: Description of Systems Simulated in This Work[a]

system	no. of oligomers	N_g	N	A (nm^2)	$\langle h \rangle$ (nm)	η_0 (cP)
S_1	74	4300	17 184	112.63	0.9831	418.62
S_2	80	3588	16 456	93.98	1.6643	298.57
S_3	78	2720	14 488	71.22	2.3888	343.40
S_4	82	2432	14 376	63.67	3.2027	215.46
S_5	95	1972	14 964	51.65	3.8417	163.50
S_6	120	2392	16 312	31.33	5.9354	33.51
S_7 (bulk)	300	34800				

[a] N_g, N, A, and $\langle h \rangle$ are the number of C atoms per each graphene sheet, the total number of atoms, surface area (of one surface), and the average surface separation, respectively.

Velocity Profiles. As explained above, in the RNEMD method the random motion of particles (heat) is turned into a directed motion (shear flow) by exchanging the momentum of

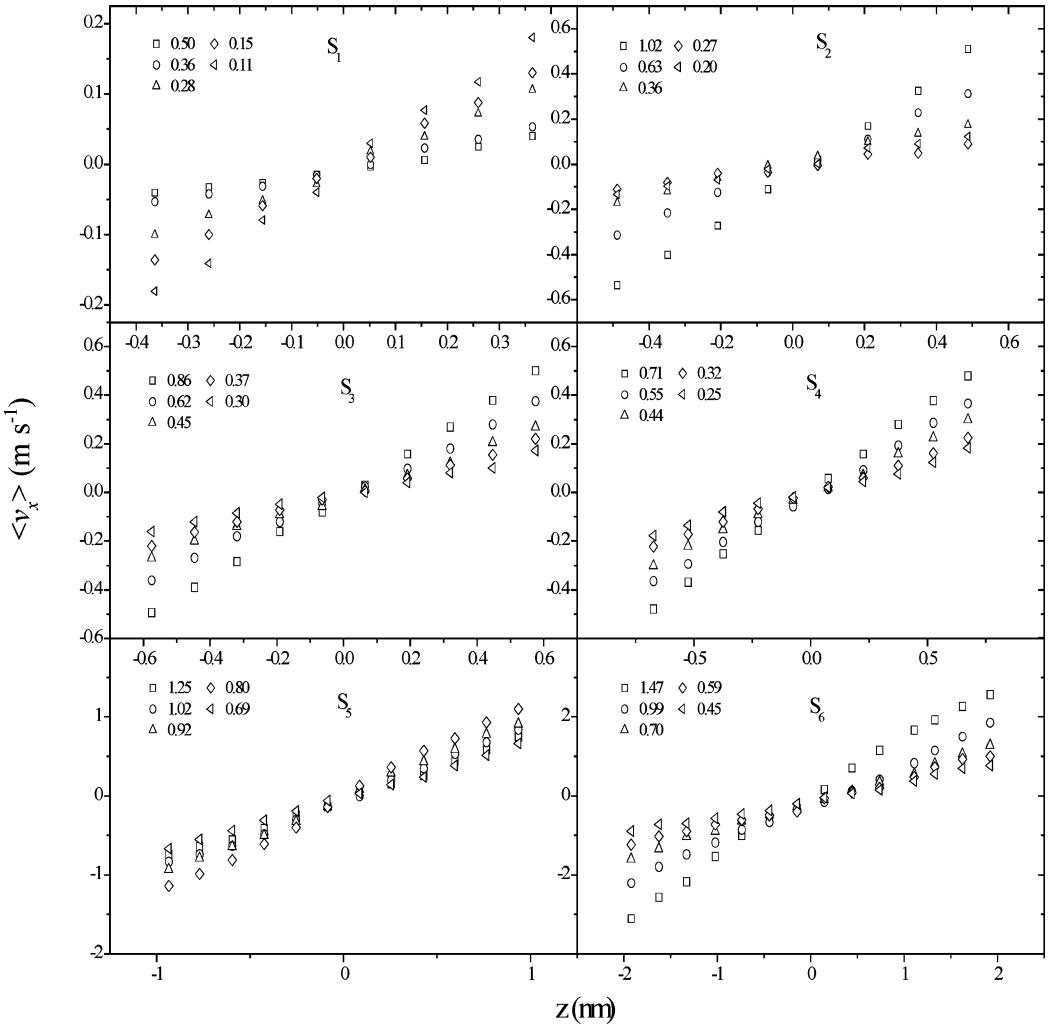

Figure 5. Velocity profiles for systems S_1-S_6. The shear rates, in 10^9 s^{-1}, are indicated in the figure.

selected atoms in the upper and lower confining surfaces. This unphysical momentum transfer leads to the development of velocity gradient in the confined fluid. In this work the distance between surfaces is divided into 10−14 thin slabs, depending on the slit width, and the *x*-components of the velocities of all atoms of a slab are time-averaged during the simulation. The number of slabs is selected so that in each slab there are a considerable number of atoms during the simulation, to get a good statistics. It is worth considering that a good linearity of the velocity profile is essential to calculate the shear viscosity. To do this, one has to carefully select the exchange frequency, or the shear rate.

Simulations were performed in the equilibrium *NAPT* ensemble, in the absence of flow, for 3 ns to generate relaxed configurations. Adjusting the proper exchange frequencies (empirically), MD simulations were performed for 5−10 ns, depending on the distance between the confining surfaces, to obtain a linear velocity profile within the polymer. After this initial time to achieve steady state, simulations were performed for another 10 ns to calculate the shear rates and the viscosity coefficients. According to continuum mechanics, for no-slip boundary conditions and Couette flow, a linear velocity profile should develop between the surfaces. Shown in Figure 5 are the linear velocity profiles for systems S_1-S_6 at different exchange frequencies. The results show linear velocity profiles for the confined fluid over the whole distance between surfaces, except for a small distance near the surfaces, at which a discontinuity in the velocity profiles is seen (not shown in Figure 5). In other words, the velocity of the fluid extrapolated to the surface position is different from the surface velocity. The discontinuity in the velocity profile at the surfaces is an indication of slip near the confining surfaces. For polymers, slip near the surfaces has already been observed in previous simulations.[49,52−60] For Couette flow, the slip length, δ, is defined as[46]

$$\delta = \frac{v_x(z = h/2) - v_x(z = -h/2)}{\gamma} \tag{6}$$

where the numerator indicates the difference between the velocities of surfaces. As a result of slip near the surfaces, a shear rate much smaller than what would be expected based on no-slip boundary conditions, $\delta = 0$, is obtained. The calculated slip length as a function of shear rate for system S_1, as a typical example, is shown in Figure 6. The results indicate that substantial slip is seen at higher shear rates. To elucidate the layering effect on the slip length, we have shown in Figure 7 the calculated slip lengths at a constant shear rate of 5.0×10^8 s^{-1}. The results show that the slip length generally decreases with increasing the distance between the surfaces. The results of Figure 7 also show that different slip behaviors are observed with variations in the surface distance. At a constant shear rate, oligomers with diffuse layers (negative solvation forces) show

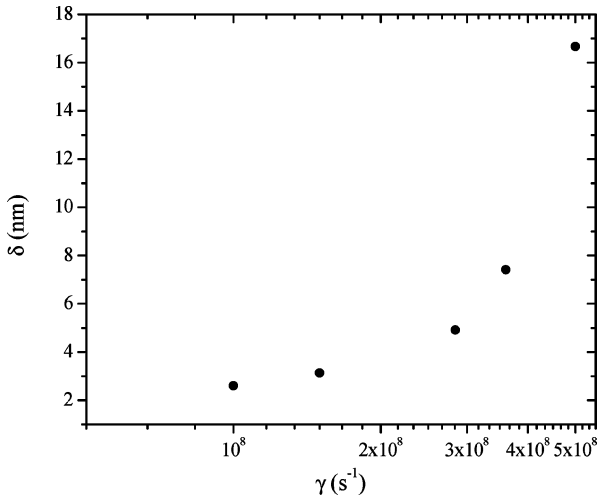

Figure 6. Slip length as a function of shear rate for system S_1.

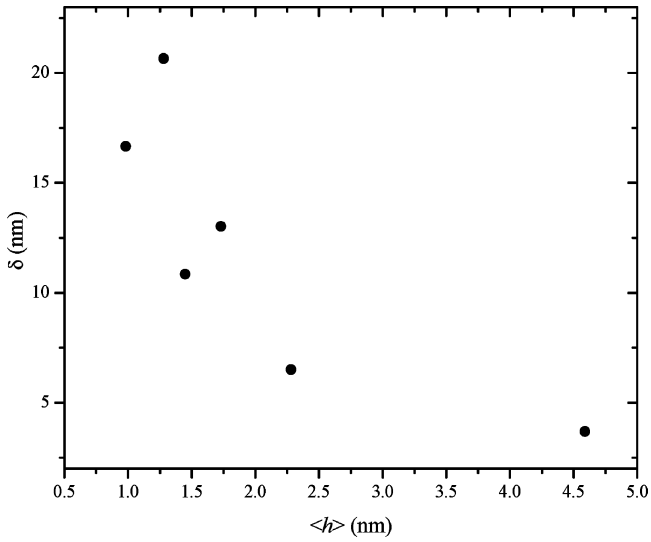

Figure 7. Slip length as a function of average surface separation at a constant shear rate, 5×10^8 s^{-1}.

a longer slip distance than the corresponding well-formed structures. In fact, there is a higher repulsive interaction between polymer and surfaces in the case of systems with a repulsive solvation force, for example, system S_1. Conversely, for system S_2, with a negative solvation force, the interaction between surfaces and polymer is weak. Therefore, oscillations in the slip distance with the distance between the surfaces can be interpreted in terms of the degree of polymer−surface interactions. This finding is in agreement with previous simulation findings of Stevens et al.,[50] who observed a velocity profile with substantial slip at the surface for weak surface−fluid interactions.

Similar to the slip distance, the slip velocity, δ', is defined as the difference between the actual surface velocities and the velocity obtained by linearly extrapolating the velocity profile to the surface positions. Shown in Figure 8 is the slip velocity as a function of shear rate, for system S_1. The results show that the slip velocity increases with increasing shear rate, a result consistent with experimental findings[84] and with previous simulation results.[43,49]

RNEMD calculations were performed for bulk PA-6,6 oligomers. Here the periodic simulation box was subdivided into slabs along the z direction and atoms inside the slab at $z = 0$ and its periodic image were propelled in the $+x$ direction, while those in slab $z = L_z/2$ and its periodic image were

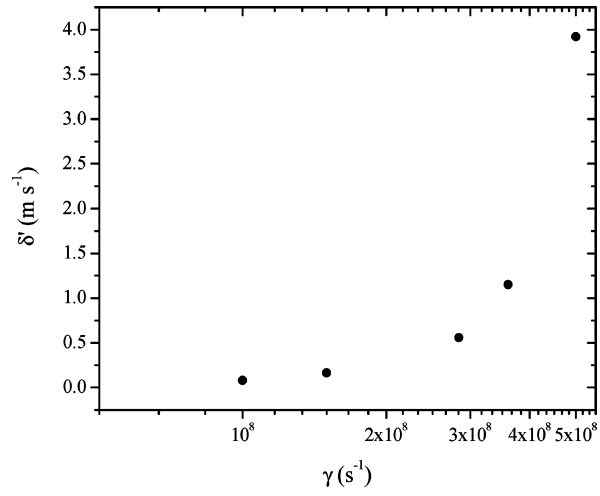

Figure 8. Slip velocity as a function of shear rate for system S_1.

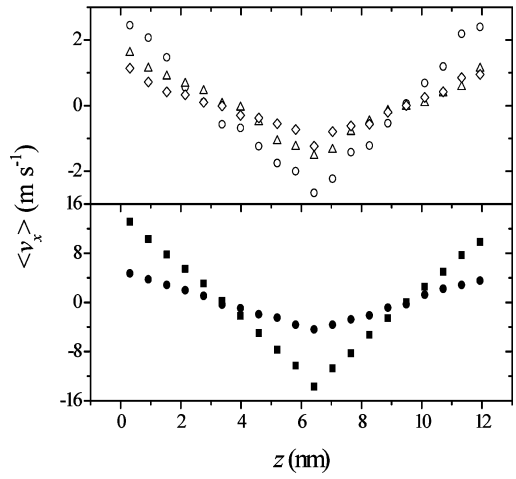

Figure 9. Velocity profiles for bulk PA-6,6. The shear rates are 4.28×10^9 s^{-1} (■), 1.51×10^9 s^{-1} (●), 8.76×10^8 s^{-1} (○), 4.64×10^8 s^{-1} (△), and 3.32×10^8 s^{-1} (◇).

propelled in the $-x$ direction. The size of the simulation cell in the z direction, L_z, was chosen bigger than those in the other two directions, to get a better statistics. The results for velocity profiles at different exchange frequencies are shown in Figure 9. As seen from the results, good linear velocity profiles are observed, even at stronger perturbations (shear rates).

Temperature Profiles. As a result of momentum transfer, friction occurs in the system. This leads to a nonuniformity in the temperature along the z-axis, which in turn causes nonuniformity in the density profile. In Figure 10 we show the temperature profiles of systems S_2 and S_3 as typical examples. The temperature profiles exhibit parabolic features (see Figure 10). At stronger perturbations, there is a bigger temperature difference between the central region of the box and the surfaces. Decreasing the perturbations, the parabolic shape of temperature profiles becomes less evident, because of the dominance of statistical fluctuations. At very weak perturbations (shear rate of 2×10^8−3×10^8 s^{-1}), the temperature difference between the hot and cold slabs is around 5 K, which is within the range of statistical fluctuations in the temperature. The results in Figure 10 also indicate a jump in the temperature at surfaces, compared to the layers of fluid beside the surfaces, which is due to the slipping of the surfaces. Moreover, our results show that for system S_2, with a negative solvation force, the temperature difference between the hot and the cold slabs is higher than that of system S_3, with a positive solvation force, at the same shear rate (see Figure 10 at 6.2×10^8 s^{-1}). Because of the stronger

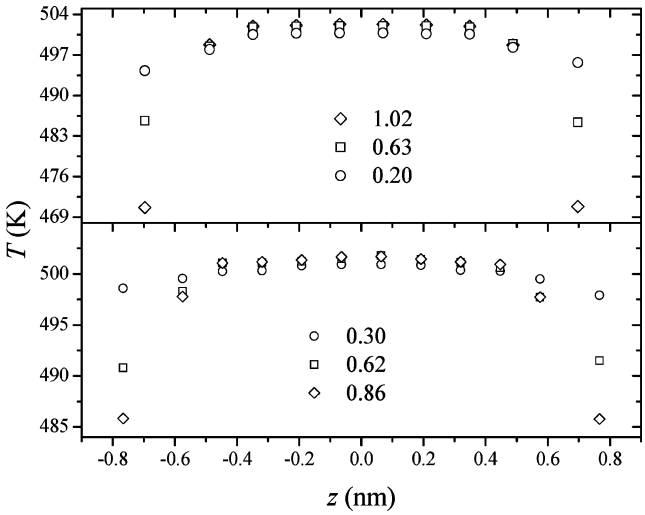

Figure 10. Temperature profiles for systems S_2 (top panel) and S_3 (bottom panel) at different shear rates. The shear rates, in 10^9 s^{-1}, are indicated in the figure.

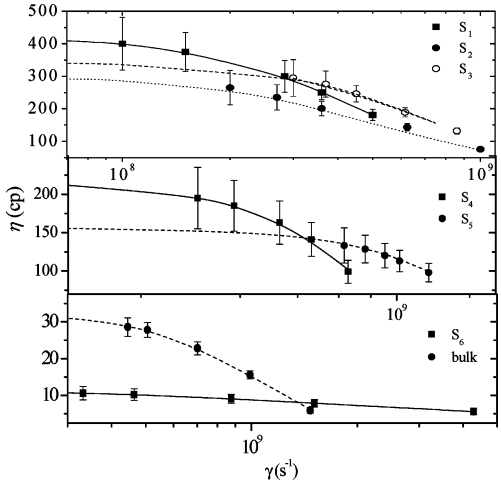

Figure 11. Shear viscosities as a function of shear rates. Solid lines represent the fit to the Carreau equation.[85] The error bars are calculated according to the method explained by Bordat and Müller-Plathe.[73]

fluid−surface interactions in system S_3, viscous heat removal by conduction to the surfaces is more efficient than that of system S_2. The development of temperature profiles, as explained above, may lead to the deviation of density profile from the equilibrium profile shown in Figure 3. Since the temperature gradient inside the confined fluid is small, our analysis (not shown) indicates no considerable deviation in the density profile of confined oligomers in the presence and absence of flow. Parabolic temperature profiles for simple fluids and bead−spring polymer models confined between walls have also been observed in previous studies by Khare et al.[44,46,49]

Shear Viscosity. For Newtonian fluids, as it is indicated in eq 2, the viscosity coefficient would be independent of the shear rate. Here we have calculated the viscosity coefficients for all shear rates, using eq 2. The results are compiled for all systems in Figure 11. From the results in Figure 11, a nonlinearity in the viscosity coefficient versus the shear rate is observable. At weaker perturbations a plateau region is observed. In this region the viscosity coefficients at zero shear rate can be obtained, by extrapolating the existing data. This extrapolation to zero shear rate requires a model. Mode-coupling theory has been extensively used for such an extrapolation.[85] An alternative approach is to employ the empirical three-parameter Carreau equation,[85] defined as

$$\eta = \frac{\eta_0}{[1 + (\lambda\gamma)^2]^{\alpha}} \tag{7}$$

to fit the viscosity as a function of shear rate. In eq 7 η_0 is the zero shear rate viscosity, λ is a characteristic time constant, and α is an exponent. This procedure has already been used by us in the case of viscosity calculation for ionic liquids.[78] We have calculated the values of η_0 for all systems, listed in Table 1. To investigate the influence of film thickness on frictional properties, the calculated results of η_0 as a function of surface distance are shown in Figure 12. Our results show that the zero shear rate viscosity increase for the confined films is due to the formation of structured layers near the surfaces. Therefore, the shear response for organized films (systems with positive solvation forces) near the surfaces corresponds to a high viscosity coefficient, as indicated in Figure 12. This finding is in agreement with experimental reports[33] and with the results of previous simulations.[16,49,52] Furthermore, our results show that the increase in viscosity with decreasing distance between surfaces shows an oscillatory behavior. This finding describes clearly that the origin of high viscosity in thin films is the formation of organized layers near the surfaces. For systems with a negative solvation force, a much lower viscosity is found with respect to what would be expected from the trend of systems with repulsive solvation forces. As the distance between the surfaces increases, the central region of box shows bulklike behavior and the viscosity does not deviate so much from the bulk fluid.

At this point, it is worth mentioning that, while our simulation is planned to mimic surface force apparatus experiments,[23−26] two distinctions are seen between the simulation and the experiment: (1) In the surface force apparatus, the viscosity is calculated from the imposed shear rate and the experimentally determined shear stress.[23−26] The shear rate is determined by assuming a linear velocity profile between the surfaces. In other words, since in the nanometric scales the velocity profile cannot be measured directly, experimental viscosities are calculated assuming no-slip boundary conditions. Our calculated results on the slip lengths and slip velocities show that this might be a rough approximation, especially, when there are weak interactions between surfaces and confined fluid. (2) The magnitude of perturbations (shear rates) in the simulation is much higher than those in the surface force apparatus.[2−26] In experimental measurement, the surfaces are moving with a velocity in the regime of 1 nm s^{-1}−1 μm s^{-1}, which means

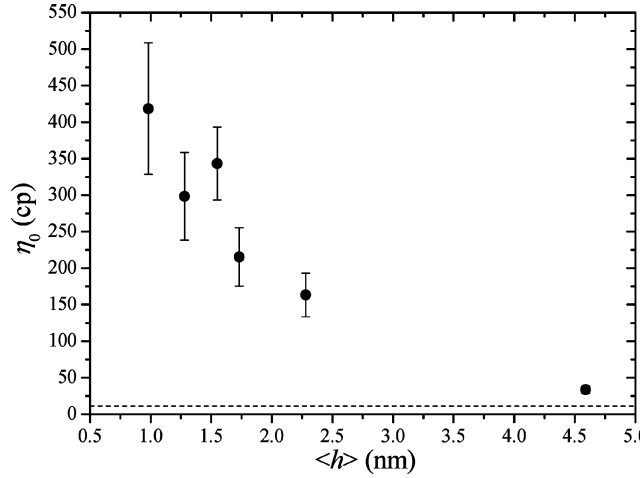

Figure 12. Average shear viscosity at zero shear rate for systems S_1−S_6 as a function of average surface separation. The dashed line indicates the viscosity coefficient of bulk PA-6,6 oligomers.

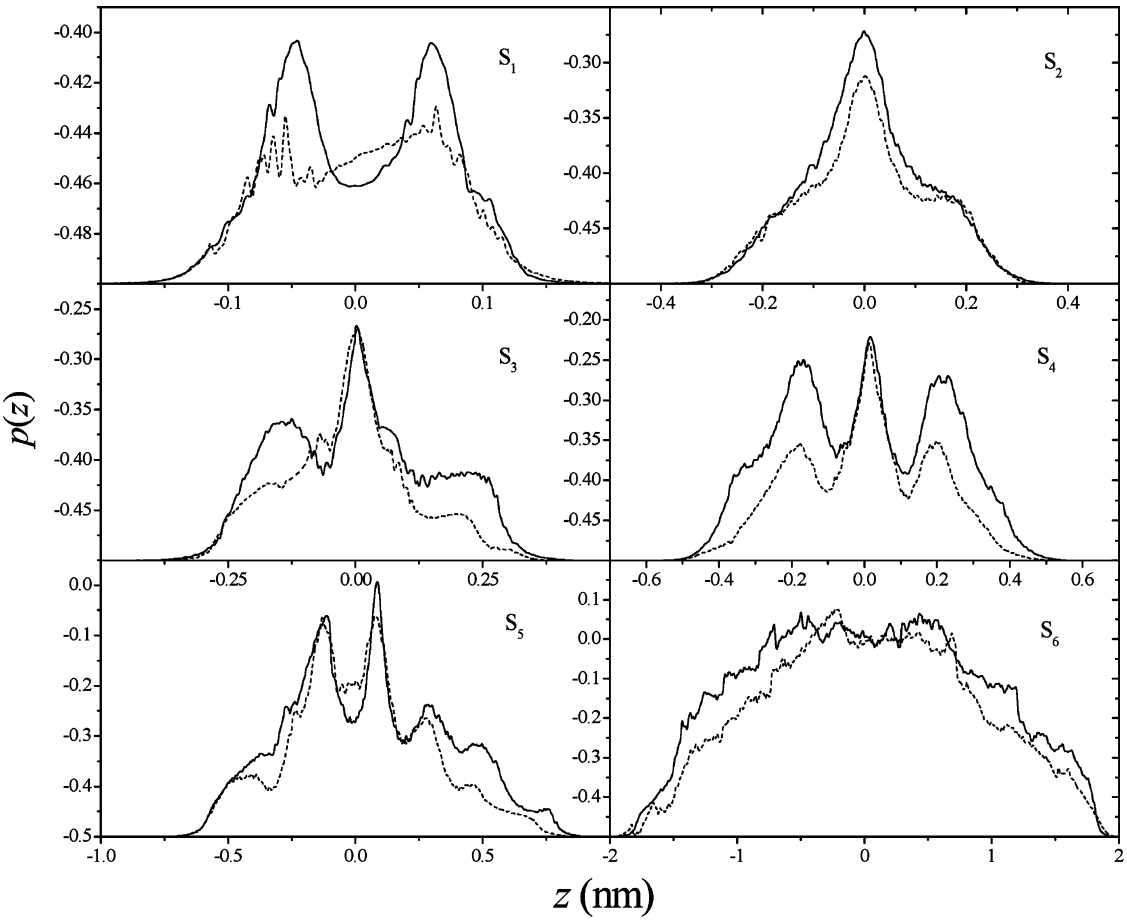

Figure 13. Orientation distribution function of end-to-end vectors with respect to surface normal as a function of their distance from the surfaces. The full curves represent the orientation distribution functions in the absence of the flow, and the dotted curves indicate the same quantity at the highest shear rates (indicated in Figure 5) imposed in this work.

that, in order to have a displacement of 1 nm in surfaces by moving the surfaces at a velocity of 1 μm s^{-1}, one has to perform simulations as long as 1 ms. This time is, of course, not achievable in the simulation. However, very recently Delhommelle and Cummings,[86] using the transient-time correlation function, could achieve shear rates comparable to experimental ones.

Flow Effect on Chain Conformations. The conformational anisotropy of oligomers under shear can be elucidated by examining the orientational distribution function (ODF) of end-to-end vectors as a function of z. The chain orientation is described by ODF in terms of the second Legendre polynomial, which is expressed as

$$p(z) = \frac{1}{2}\langle 3(\mathbf{u}_i \cdot \mathbf{u}_j)^2 - 1\rangle \qquad (8)$$

where $\mathbf{u}_i$ and $\mathbf{u}_j$ are unit vectors and p is the second Legendre polynomial. In order to calculate the orientations with respect to the surfaces, one of the unit vectors is taken as the surface normal, z. Here, the second Legendre polynomial shows the orientation of the end-to-end vector along the z direction and varies between -0.5, in the case of perpendicular alignment, and 0.5 in the case of parallel alignment, with a zero value indicating random alignment with respect to the surface normal. In Figure 13, the preferential orientations of end-to-end vectors with respect to the z-axis, at different shear rates, are shown. As the results show, the end-to-end vectors show perpendicular orientation, with respect to surface normals, at short distances from the surfaces, even in the absence of flow, as a result of the spacial confinement, as shown in our former work.[1] Increasing the distance between surfaces causes more randomness in the end-to-end vector alignment. In systems S_5 and S_6 end-to-end vectors orient randomly in the central region of the box. The results in Figure 13 show that, in the presence of flow, the end-to-end vectors are more oriented parallel to the surfaces (the flow plain). In very short distances from surfaces, because of the strong effects of surfaces, the orientation does not depend so much on the absence or the presence of flow. At larger distances from the confining surfaces, the flow increases the orientation of end-to-end vectors, compared to the stationary fluid.

Conclusions

The RNEMD technique[63,72−78] is employed to calculate the shear viscosity of nanoconfined PA-6,6 oligomers, confined between graphene surfaces. Our results show that by applying the RNEMD method[63,72−78] to shear the confining surfaces, linear velocity profiles are obtained in the confined fluid. It is shown that substantial slip occurs at the surfaces, with the slip distance depending on the shear rate and on the magnitude of fluid−surface interactions. At surface separations corresponding to well-formed layers between the surfaces, the slip distance is shorter. Therefore, the slip distance shows oscillatory behavior with out-of-phase oscillations with respect to the solvation force oscillations. The same behavior is observed for slip velocity. Our results also show that shearing the surfaces causes the development of a parabolic temperature profile in the system. In this case the difference in the temperature of the cold slabs (surfaces)

and the hot slab (center of fluid) depends on the shear rate and on the layering effect. Well-formed oligomer layers can conduct the viscous heat more easily, and hence, a lower temperature difference is seen between the cold and the hot slabs. The calculated viscosity coefficients show strong shear rate dependence. The zero shear rate viscosity coefficients of the confined fluid increase considerably with reducing the surface separations. Moreover, the zero shear rate viscosities show oscillatory patterns with maxima corresponding to solvation force maxima. Analysis of chain conformations shows that the chains adopt a more oriented conformation in the presence of flow. Moreover, with increasing shear rate, the chains adopt more preferential orientations parallel to the surfaces (flow plain).

Acknowledgment. The support of this work by the Excellence Cluster Center of Smart Interfaces at the Technische Universität Darmstadt is gratefully acknowledged.

References and Notes

(1) Eslami, H.; Müller-Plathe, F. *J. Phys. Chem. B* **2009**, *113*, 5568.
(2) Persson, B. N. J. *Sliding Friction: Physical Principles and Applications*, 2nd ed.; Springer: Heidelberg, 2000.
(3) Dowson, D. *History of Tribology*, 2nd ed.; Professional Engineering Publishing: London and Bury St Edmunds, 1998.
(4) Tadmor, R.; Janik, J.; Klein, J.; Fetters, L. J. *Phys. Rev. Lett.* **2003**, *91*, 115503.
(5) Donnet, C.; Erdemir, A. *Surf. Coat. Technol.* **2004**, *76*, 180.
(6) Vorvolakos, K.; Chaudhury, M. *Langmuir* **2003**, *19*, 6778.
(7) Persson, B. N. J.; Volokitin, A. I. *Eur. Phys. J. E* **2006**, *21*, 69.
(8) Cayer-Barrioz, J.; Mazuyer, D.; Tonck, A.; Yamaguchi, E. *Langmuir* **2009**, *25*, 10802.
(9) Bitsanis, J.; Somars, S. A.; Davis, H. T.; Tirrell, M. *J. Chem. Phys.* **1990**, *93*, 3427.
(10) Robbins, M. O.; Thompson, P. A. *Science* **1991**, *253*, 916.
(11) Ribarsky, M. W.; Landman, U. *J. Chem. Phys.* **1992**, *97*, 1937.
(12) Gupta, S.; Koopman, D. C.; Westerman-Clark, G. B.; Bitsanis, I. A. *J. Chem. Phys.* **1994**, *100*, 8444.
(13) Ouyang, J.; Luedtke, W. D.; Landman, U. *Bull. Am. Phys. Soc.* **1995**, *40*, 425.
(14) Gao, J.; Luedtke, W. D.; Landman, U. *J. Chem. Phys.* **1997**, *106*, 4309.
(15) Curry, J. E. *J. Chem. Phys.* **2000**, *113*, 2400.
(16) Cui, S. T.; Cummings, P. T.; Cochran, H. D. *J. Chem. Phys.* **2001**, *114*, 7189.
(17) Choudhury, N.; Pettitt, B. M. *J. Am. Chem. Soc.* **2005**, *127*, 3556.
(18) Marti, J.; Nagy, G.; Gordillo, M. C.; Guardia, E. *J. Chem. Phys.* **2006**, *124*, 094703.
(19) Davis, H. T. *Chem. Eng. Commun.* **1987**, *58*, 413.
(20) Vanderlick, T. K.; Davis, H. T. *J. Chem. Phys.* **1987**, *87*, 1791.
(21) Somers, S. A.; Davis, H. T. *J. Chem. Phys.* **1992**, *96*, 5389.
(22) Bitsanis, I.; Vanderlick, T. K.; Tirell, M.; Davis, H. T. *J. Chem. Phys.* **1988**, *89*, 3152.
(23) Bhushan, B.; Israelachvili, J. N.; Landman, U. *Nature* **1995**, *374*, 607.
(24) Israelachvili, J. N.; McGuiggan, P. M.; Homola, A. M. *Science* **1988**, *240*, 189.
(25) Klein, J.; Kumacheva, E. *Science* **1995**, *269*, 816.
(26) Klein, J.; Kumacheva, E. *J. Chem. Phys.* **1998**, *108*, 7010.
(27) Drummond, C.; Israelachvili, J.; Richetti, P. *Phys. Rev. E* **2003**, *67*, 066110.
(28) Georges, E.; Georges, J.-M.; Hollinger, S. *Langmuir* **1997**, *13*, 3454.
(29) Georges, J.-M.; Millot, S.; Tonck, A.; Coy, R. C.; Schlijper, A. G.; Williamson, B. P. *Tribology for Energy Conservation*; Dowson, D., et al., Eds.; Tribology Series 32; Elsevier: Amsterdam, 1998; p 51.
(30) Gourdon, D.; Israelachvili, J. N. *Phys. Rev. E* **2003**, *68*, 021602.
(31) Tadmor, R.; Janick, J.; Klein, J.; Fetters, L. *Phys. Rev. Lett.* **2003**, *91*, 115503.
(32) Bureau, L. *Macromolecules* **2007**, *40*, 9197.
(33) Bae, S. C.; Granick, S. *Annu. Rev. Phys. Chem.* **2007**, *58*, 353.
(34) Buenviaje, C.; Ge, S.; Rafailovich, M.; Sokolov, J.; Drake, J. M.; Overney, R. M. *Langmuir* **1999**, *15*, 6446.
(35) Shin, K.; Obukhov, S.; Chen, J.; Huh, J.; Hwang, Y.; Mok, S.; Dobriyal, P.; Thiyagarajan, P.; Russel, T. P. *Nature* **2007**, *6*, 961.
(36) Anderson, J. D., Jr. *Computational Fluid Dynamics, The Basics with Applications*; McGraw-Hill: New York, 1995.
(37) Jabbarzadeh, A.; Atkinson, J. D.; Tanner, R. I. *Tribol. Int.* **2002**, *35*, 35.
(38) Trozzi, C.; Ciccotti, G. *Phys. Rev. A* **1984**, *29*, 916.
(39) Bitsanis, I.; Magda, J. J.; Tirrell, M.; Davis, H. T. *J. Chem. Phys.* **1987**, *87*, 1733.
(40) Bitsanis, I.; Somers, S. A.; Davis, H. T.; Tirrell, M. *J. Chem. Phys.* **1990**, *93*, 3427.
(41) Thompson, P. A.; Robbins, M. O. *Phys. Rev. A* **1990**, *41*, 6830.
(42) Thompson, P. A.; Grest, G. S.; Robbins, M. O. *Phys. Rev. Lett.* **1992**, *68*, 3448.
(43) Manias, E.; Hadziioannou, G.; Bitsanis, I.; Ten Brinke, G. *Europhys. Lett.* **1993**, *24*, 99.
(44) Khare, R.; de Pablo, J. J.; Yethiraj, *J. Chem. Phys.* **1997**, *107*, 2589.
(45) Khare, R.; de Pablo, J. J.; Yethiraj, *J. Chem. Phys.* **2001**, *114*, 7593.
(46) Khare, R.; Keblinski, P.; Yethiraj, *Int. J. Heat Mass Transfer* **2006**, *49*, 3401.
(47) Manias, E.; Bitsanis, I.; Hadziioannou, G.; Brinke, G. *Europhys. Lett.* **1996**, *33*, 371.
(48) Manias, E.; Hadziioannou, G.; Brinke, G. *J. Chem. Phys.* **1994**, *101*, 1721.
(49) Khare, R.; de Pablo, J. J.; Yethiraj, A. *Macromolecules* **1996**, *29*, 7910.
(50) Stevens, M. J.; Mondello, M.; Grest, G. S.; Gui, S. T.; Cochran, H. D.; Cummings, P. T. *J. Chem. Phys.* **1997**, *106*, 7303.
(51) Balasundarama, R.; Jianga, S.; Belak, J. *Chem. Eng. J.* **1999**, *74*, 117.
(52) Jabbarzadeh, A.; Harrowell, P.; Tanner, R. I. *Phys. Rev. Lett.* **2005**, *94*, 126103.
(53) Jabbarzadeh, A.; Atkinson, J. D.; Tanner, R. I. *Phys. Rev. E* **2000**, *61*, 690.
(54) Jabbarzadeh, A.; Atkinson, J. D.; Tanner, R. I. *J. Non-Newtonian Fluid Mech.* **1998**, *77*, 53.
(55) Jabbarzadeh, A.; Atkinson, J. D.; Tanner, R. I. *Comput. Phys. Commun.* **1997**, *107*, 123.
(56) Jabbarzadeh, A.; Atkinson, J. D.; Tanner, R. I. *J. Chem. Phys.* **1999**, *110*, 2612.
(57) Gui, S. T.; McCabe, C.; Cummings, P. T.; Cochran, H. D. *J. Chem. Phys.* **2003**, *118*, 8941.
(58) Jeng, Y.; Chen, C.; Shyu, S. *Tribol. Lett.* **2003**, *15*, 293.
(59) Müller, M.; Pastorino, C.; Servantie, J. *J. Phys.: Condens. Matter* **2008**, *20*, 494225.
(60) Zhang, J.; Hansen, J. S.; Todd, B. D.; Daivis, P. J. *J. Chem. Phys.* **2007**, *126*, 144907.
(61) Goujon, F.; Malfrey, P.; Tildesley, D. J. *Macromolecules* **2009**, *42*, 4310.
(62) Eslami, H.; Mozaffari, F.; Moghadasi, J.; Müller-Plathe, F. *J. Chem. Phys.* **2008**, *129*, 194702.
(63) Müller-Plathe, F. *Phys. Rev. E* **1999**, *59*, 4894.
(64) Müller, T. J.; Al-Samman, M.; Müller-Plathe, F. *J. Chem. Phys.* **2008**, *129*, 014102.
(65) Snook, I. K.; Van Megan, W. *J. Chem. Phys.* **1980**, *72*, 2907.
(66) Schoen, M.; Diestler, D. J.; Cushman, J. H. *J. Chem. Phys.* **1994**, *100*, 7707.
(67) Schoen, M.; Diestler, D. J.; Cushman, J. H. *Phys. Rev. B* **1993**, *47*, 5603.
(68) Schoen, M.; Diestler, D. J.; Cushman, J. H. *J. Chem. Phys.* **1987**, *87*, 5464.
(69) van Megen, W. J.; Snook, I. K. *J. Chem. Phys.* **1981**, *74*, 1409.
(70) Allen, M. P.; Tildesley, D. J. *Computer Simulation of Liquids*; Clarendon Press: Oxford, 1987.
(71) Evans, D. J.; Morriss, G. P. *Statistical Mechanics of Nonequilibrium Liquids*; Academic: London, 1990.
(72) Müller-Plathe, F.; Reith, D. *Comput. Theor. Polym. Sci.* **1999**, *9*, 203.
(73) Bordat, P.; Müller-Plathe, F. *J. Chem. Phys.* **2002**, *116*, 3362.
(74) Zhang, M.; Lussetti, E.; de Souza, L. E. S.; Müller-Plathe, F. *J. Phys. Chem. B* **2005**, *109*, 15060.
(75) Zhang, M.; Müller-Plathe, F. *J. Chem. Phys.* **2005**, *123*, 124502.
(76) Cavalcanti, W. L.; Chen, X. Y.; Müller-Plathe, F. *Phys. Status Solidi A* **2007**, *204*, 935.
(77) Chen, X. Y.; Carbone, P.; Cavalcanti, W. L.; Milano, P.; Müller-Plathe, F. *Macromolecules* **2007**, *40*, 8087.
(78) Zhao, W.; Leroy, F.; Balasubramanian, S.; Müller-Plathe, F. *J. Phys. Chem. B* **2008**, *112*, 8129.
(79) Müller-Plathe, F. *Comput. Phys. Commun.* **1993**, *78*, 77.
(80) Tarmyshov, K.; Müller-Plathe, F. *J. Chem. Inf. Model.* **2005**, *45*, 1943.
(81) Goudeau, S.; Charlot, M.; Vergelati, C.; Müller-Plathe, F. *Macromolecules* **2004**, *37*, 8072.
(82) Goudeau, S.; Charlot, M.; Müller-Plathe, F. *J. Phys. Chem. B* **2004**, *108*, 18779.
(83) Berendsen, H. J. C.; Postma, J. P. M.; van Gunsteren, W. F.; DiNola, A.; Haak, J. R. *J. Chem. Phys.* **1984**, *81*, 3684.
(84) Migler, K. B.; Hervet, H.; Leger, L. *Phys. Rev. Lett.* **1993**, *70*, 287.
(85) Kellar, M. S.; Maginn, E. J. *J. Phys. Chem. B* **2007**, *111*, 4867.
(86) Delhommelle, J.; Cummings, P. T. *Phys. Rev. B* **2005**, *72*, 172201.

JP908659W